pubs.acs.org/Biomac

Article

Insights into the Mechanism of Protein Loading by Chain-Length Asymmetric Complex Coacervates

Eugenia Apuzzo, Marilina Cathcarth, Agustín S. Picco, Catalina von Bilderling, Omar Azzaroni, Maximiliano L. Agazzi,* and Santiago E. Herrera*

Cite This: https://doi.org/10.1021/acs.biomac.4c01516

Read Online

ACCESS | Metrics & More | Article Recommendations | Supporting Information

ABSTRACT: The study of the phase behavior of polyelectrolyte complex coacervates has attracted significant attention in recent years due to their potential use as membrane-less organelles, microreactors, and drug delivery platforms. In this work, we investigate the mechanism of protein loading in chain-length asymmetric complex coacervates composed of a polyelectrolyte and an oppositely charged multivalent ion. Unlike the symmetric case (polycation + polyanion), we show that protein loading is highly selective based on the protein's net charge: only proteins with charges opposite to the polyelectrolyte can be loaded. Through a series of systematic experiments, we identified that the protein loading process relies on the formation of a neutral three-component coacervate in which both the protein and the multivalent ion serve as complexing agents for the polyelectrolyte. Lastly, we demonstrated that this mechanism extends to the sequestration of other charged small molecules, offering valuable insights into designing functional multicomponent coacervates.

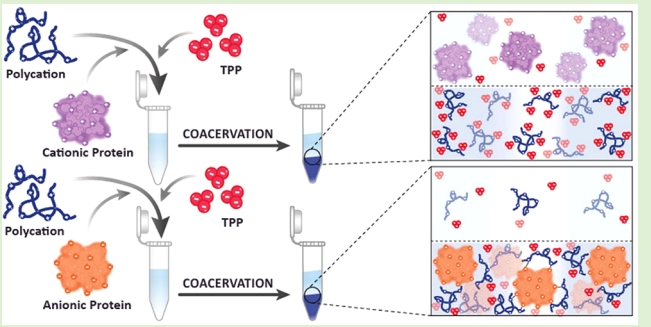

1. INTRODUCTION

Protein encapsulation is a rapidly growing area of interest in various fields, such as biomedicine, food technology, biocatalysis, environmental remediation, and protocell research.[1,2] While polymeric materials are increasingly employed for protein encapsulation, traditional synthesis methods often necessitate organic solvents, posing risks of protein damage while also escalating manufacturing costs and compromising sustainability.[3,4] In this context, complex coacervates have emerged as attractive and versatile platforms for encapsulating biomacromolecules, thanks to their facile and entirely aqueous fabrication processes.[5,6]

Complex coacervates are viscoelastic materials formed through the interaction of oppositely charged polyelectrolytes in aqueous solutions.[7−9] They internally consist of a dense mixture of polyelectrolytes linked by intrinsic and extrinsic ionic pairs and water molecules.[10] The phase behavior of the symmetric case, where ionization degree, chain length, and concentrations of the two polyelectrolytes are equal, has been extensively characterized.[11−13] Because coacervation is essentially a charge-driven process, electrostatic interactions play a crucial role in determining the degree of partitioning of molecules into the dense phase of the coacervate.[14,15] Thus, coacervates can be loaded with a wide range of charged cargos, including therapeutic drugs, food additives, peptides, nucleic acids, and metabolites.[7−17] The ability to sequester and compartmentalize ionic biomolecules, along with the existence of intracellular condensates formed by liquid−liquid phase separation of biomolecules (such as proteins, nucleic acids, and metabolites), has led to the study of complex coacervates as biomimetic models for understanding cellular processes.[18−21]

In this context, a particularly interesting case involves using the process of coacervation to sequester proteins, as they can carry a net charge when the pH is sufficiently distant from their isoelectric point.[22,23] Given the possibility of proteins to present numerous charges, the ability of a protein to induce complex coacervation when combined with an oppositely charged polymer has been studied in recent years.[24−26] However, achieving liquid−liquid phase separation via this method requires both high protein concentrations and a substantial net charge threshold.[3,27,28] As such, the experimental conditions required for this type of coacervation may not be favorable for practical uses.

In the past decade, ternary coacervate systems have been reported as an effective strategy for encapsulating proteins, where the protein of interest forms complexes with a mixture of cationic and anionic polyelectrolytes.[2,3,29] Unlike binary

Received: October 31, 2024
Revised: December 31, 2024
Accepted: January 3, 2025

protein/polyelectrolyte systems, for this approach, protein concentration and charge are not crucial to inducing coacervation. The protein encapsulation based on ternary complexes encompasses the following mechanism: 1) initial formation of an intermediary complex between the protein and an oppositely charged polyelectrolyte, and 2) subsequent coacervation induced by the introduction of a second polyelectrolyte, which interacts directly with the intermediary complex.[4] Recently, Perry and Blocher Mctigue established foundational principles predicting the experimental conditions for successful protein incorporation into ternary coacervates.[30] Specifically, they conducted loading experiments with different proteins (spanning a wide range of isoelectric points) using a chain-length-symmetrical polylysine/polyglutamate system, varying the molar charge ratio between polyelectrolytes. Key findings of this work suggest that maximum protein loading occurs near the point where positive and negative charge fractions equalize. Additionally, when proteins carry a net charge, optimal encapsulation is achieved with a slight excess of the polyelectrolyte opposite to the protein's charge.[3,4]

While coacervate complexes are commonly associated with polycations and polyanions, our recent research demonstrates that replacing one polymeric building block with a sufficiently charged small molecule or multivalent ion (e.g., potassium ferricyanide) yields liquid coacervates with phase diagrams closely resembling those of symmetric cases.[31] This suggests that a polyelectrolyte/multivalent ion system can be considered a special case of coacervate with high chain length asymmetry. The most popular asymmetric coacervates are those based on polyamines cross-linked with phosphate-based anions.[7,32,33] While these one-polyelectrolyte coacervate systems have been utilized as platforms for protein loading,[6,34] there is a lack of comprehensive studies on the principles and parameters governing the encapsulation processes. The understanding of the sequestration processes of biomolecules by asymmetric systems is not only important for the technological application of coacervate platforms but also for the biomimetic study of cellular mechanisms mediated by asymmetric coacervates such as protocells.[14,35,36] This becomes particularly relevant when considering that multicomponent asymmetric coacervates offer more realistic models for mimicking cellular condensates compared to symmetric complexes.[37−39]

In general, polyamine/multivalent anion complexes have demonstrated encapsulation of negatively charged proteins, activated by the interaction between the biomacromolecule and the polycation.[6,40,41] For instance, Lapitsky and colleagues investigated the loading properties of complexes of chitosan/tripolyphosphate (TPP) using two model proteins with anionic character at the working pH (5.5 and 6): bovine serum albumin (BSA, pI 4.7−4.9) and α-lactalbumin (pI 4.2−4.5).[34] They noted that the complexes efficiently encapsulated anionic proteins under specific experimental conditions and observed a linear increase in encapsulation efficiency with the production yield of complexes. In parallel, they also evaluated the encapsulation of BSA at pH 4, where the protein carries a net positive charge, finding that the encapsulation efficiency stayed below 10% due to the elimination of electrostatic interaction between chitosan and the protein.

While these studies may provide information on the uptake properties of asymmetric complexes, the use of a few model proteins does not allow for a comprehensive understanding. On the other hand, uptake behaviors have always been explored using the polyamine/multivalent anion system without considering the opposite asymmetric combination: polyanion/multivalent cation. Considering this, we postulate the following questions: (a) How do asymmetric coacervates load proteins or other charged molecules? (b) What differences exist between the symmetric and asymmetric responses to protein uptake? (c) Is it possible to establish precise guidelines for loading proteins in asymmetric coacervates? To address these questions, we selected poly(allylamine)/tripolyphosphate (PAH/TPP) complexes as a model of asymmetric coacervates to encapsulate a wide range of proteins at pH 7.4. Additionally, we compared this system with a reverse asymmetric complex based on the complexation of poly(acrylic acid) (PAA) with tetraethylenepentamine (TEPA) as a model multivalent cationic molecule. Through an extensive set of physicochemical studies, we corroborated that protein encapsulation in asymmetric coacervates preferably occurs when the protein's charge is opposite to that of the polyelectrolyte. Furthermore, maximum complexation efficiency is achieved with a slight excess of polyelectrolyte in the mixture. By quantifying the three components in the coacervate phase (polyelectrolyte, multivalent ion, and protein) as a function of the analytical concentration of the multivalent ion, we propose that protein sequestration involves the formation of a ternary complex, in which multivalent ions and proteins synergistically act as complexing agents for the polyelectrolyte. When the multivalent ion is in excess, it displaces the protein, leading to a decreased loading efficiency. These observations align with previous findings and suggest a potentially universal mechanism that can be applied to proteins and other charged molecules. Thus, asymmetric coacervate systems may function as selective sequesters of charged molecules. The results obtained provide a comprehensive understanding of protein partitioning processes in asymmetric coacervates, which can be useful for application as encapsulation and separation platforms, as well as artificial membrane-less organelles.

2. MATERIALS AND METHODS

2.1. Materials. Sodium tripolyphosphate (TPP), potassium ferricyanide, pentaamminechlororuthenium(III) chloride, poly(allylamine hydrochloride) (PAH, Mw ∼ 17500), poly(fluorescein isothiocyanate allylamine hydrochloride) (PAH-FITC, Mw ∼ 56000), poly(acrylic acid) (PAA, Mw ∼ 450000), tetraethylenepentamine (TEPA), 4-(2-hydroxyethyl)-1-piperazineethanesulfonic acid (HEPES), albumin from chicken egg white (OVA), glucose oxidase from *Aspergillus niger* (GOx), bovine serum albumin (BSA), hemoglobin human (Hb), cytochrome c from equine heart (Cit-C) and lysozyme from chicken egg white (HEWL) were purchased from Sigma-Aldrich. Sodium hydroxide and hydrochloric acid were purchased from Anedra. All chemicals were used without further purification.

2.2. Preparation of TPP/PAH Complex Coacervates. The PAH/TPP coacervates were prepared by mixing both components dissolved in HEPES (pH 7.4), using the procedure described below. Two stock solutions of TPP (10 mM) and PAH (20 mM, monomeric concentration) were prepared using 50 mM HEPES buffer at pH 7.4 as the solvent, with small amounts of 1 M HCl and 1 M NaOH added to counteract potential pH variations caused by the dissolution of solids. To prepare a coacervate sample, a given volume (V_{buffer}) of 50 mM HEPES buffer (pH = 7.4) was placed in a beaker containing a magnetic stir bar (2 cm), followed by a volume (V_{PAH}) of PAH stock solution, and finally a volume (V_{TPP}) of TPP stock

https://doi.org/10.1021/acs.biomac.4c01516
Biomacromolecules XXXX, XXX, XXX−XXX

solution. The entire procedure was conducted with constant stirring (100 rpm) at room temperature, with 5-min intervals between additions. For simplicity, we will hereafter refer to C_{PAH} as the analytical concentration of PAH expressed in monomer concentration, i.e., the total sum of NH_2 and NH_3^+ concentrations. For the preparation of each coacervate sample, C_{PAH} was set at 1.5 mM to maintain a constant total polyelectrolyte concentration, regardless of the variation in the molar ratio of C_{TPP}/C_{PAH}. Thus, the TPP concentration (C_{TPP}) varied in each sample according to the pre-established C_{TPP}/C_{PAH} ratio. While this was the protocol used for most experiments, in cases where C_{PAH} differed from 1.5 mM (particularly those solutions with very high C_{PAH}), higher concentration stock solutions of PAH and TPP were used.

2.3. Preparation of PAH/Protein/TPP Complex Coacervates. To obtain 2 mL of PAH/Protein/TPP coacervates, the following solutions were sequentially mixed in a 5 mL beaker with constant stirring (100 rpm): (1) 50 mM HEPES pH 7.4, (2) 150 μL of PAH (20 mM in HEPES buffer), (3) 250 μL of protein (2 mg/mL in HEPES buffer), and (4) TPP (10 mM in HEPES buffer). The volumes of HEPES and TPP were adjusted according to the value of C_{TPP}/C_{PAH}. Similarly to the previous case, a 5-min interval was allowed between each addition step. The final concentrations of PAH and protein in the mixture were always 1.5 mM and 0.25 mg/mL, respectively. The obtained mixture was aged for 24 h at room temperature. The protein loading efficiency, expressed as a percentage, was evaluated by analyzing the protein content in the liquid phase (supernatant) after centrifuging the sample for 20 min at 10,000 rpm (14,000 × g). The bicinchoninic acid colorimetric assay (BCA kit, Thermo Fisher) was used to quantify the protein in the supernatant. The procedure was repeated three times for each of the evaluated conditions.

The loading efficiency was calculated as

$$\%\text{Loading efficiency} = ((C_{protein} - C_{protein,supernatant})/C_{protein}) \times 100$$

2.4. PAA/Protein/TEPA Coacervates Preparation. PAA/Protein/TEPA complex coacervates were prepared following the same protocol for the preparation of PAH/Protein/TPP complex coacervates, but replacing the 20 mM PAH and the 10 mM TPP stock solutions with 20 mM PAA and 10 mM TEPA stock solutions (both prepared in HEPES buffer at pH 7.4), respectively.

2.5. PAH/$[Fe(CN)_6]^{3-}$/TPP and PAH/$[Ru(NH_3)_6]^{3+}$/TPP Coacervates Preparation. PAH/X/TPP complex coacervates (X = $[Fe(CN)_6]^{3-}$ or $[Ru(NH_3)_6]^{3+}$) were obtained by sequential mixing of (1) PAH, (2) X, (3) water, and (4) TPP stock solutions, as in the case of the PAH/BSA/TPP system. Stock solutions of PAH, X, and TPP were prepared in HEPES buffer at pH = 7.4 in concentrations of 40 mM, 10 mM, and 10 mM, respectively. For the preparation of 2 mL of PAH/$[Fe(CN)_6]^{3-}$/TPP complex coacervate solution (C_{PAH} = 10 mM, $C_{Ferricyanide}$ = 0.5 mM), the following volumes of stock solutions were mixed: V_{PAH} = 0.5 mL; $V_{Ferricyanide}$ = 0.1 mL; V_{water} = (2 mL − V_{PAH} − $V_{Ferricyanide}$ − V_{TPP}); V_{TPP} = 2 mL × C_{TPP}/C_{PAH}. For the preparation of 2 mL of PAH/$[Ru(NH_3)_6]^{3+}$/TPP complex coacervate solution (C_{PAH} = 10 mM, $C_{Hexaammineruthenium(III)}$ = 2 mM), the following volumes of stock solutions were mixed: V_{PAH} = 0.5 mL; $V_{Hexaammineruthenium(III)}$ = 0.4 mL; V_{water} = (2 mL − V_{PAH} − $V_{Hexaammineruthenium(III)}$ − V_{TPP}); V_{TPP} = 2 mL × C_{TPP}/C_{PAH}. The loading efficiency of X, expressed as a percentage, was evaluated by analyzing the concentration of X in the liquid phase (supernatant) after centrifuging the sample for 20 min at 10,000 rpm (14,000 × g). C_X,supernatant was determined by UV−vis spectroscopy by means of a calibration curve at λ_{max} (427 nm for $[Fe(CN)_6]^{3-}$, and 288 nm for $[Ru(NH_3)_6]^{3+}$). The procedure was repeated three times for each value of C_{TPP}/C_{PAH} and the loading efficiency was calculated as

$$\%\text{Loading efficiency} = ((C_X - C_{X,supernatant})/C_X) \times 100$$

2.6. Turbidity Measurements. To investigate the influence of BSA on the coacervation of PAH/TPP, turbidity measurements were employed to qualitatively monitor the degree of coacervation as a function of the C_{TPP}/C_{PAH}. Briefly, a 2 mL sample was prepared within a plastic tube and immediately vortexed. Then, it was quickly placed into a plastic cuvette (1 cm optical path length) and the absorbance was read at 500 nm with a PerkinElmer Lambda 35 spectrophotometer. This procedure was conducted in triplicate for each of the evaluated conditions. Turbidity was expressed as absorbance at 500 nm. A sample containing 50 mM HEPES in deionized water was used as reference.

2.7. Optical Microscopy Measurements. Microscopy observations were made with an inverted microscope (BIM500FL, Bioimager, ON, Canada). Samples were prepared in 1.5 mL microcentrifuge tubes and immediately used for microscopy observations (for each sample, 20 μL of the as-prepared coacervate dispersion was placed on top of a glass slide). Images were collected using a 100× magnification objective with oil immersion (Carl Zeiss CP ACHROMAT 40×; Carl Zeiss CP ACHROMAT 100×, NA = 1.25).

2.8. Quantification of Components within the PAH/TPP and PAH/Protein/TPP Coacervates. The partitioning of components (PAH, TPP, and BSA) within both dense and liquid coacervate phases was studied by quantifying the amount of each component in the supernatant after centrifugation (10000 rpm, 14,000 × g). All samples were prepared as previously described and stored at room temperature for 24 h prior to centrifugation. The BSA content in the supernatant was obtained following the protocol described previously. The PAH and TPP contents were obtained as described in the following. For each condition, quantifications were performed on three samples obtained using the same protocol.

2.8.1. Quantification of PAH. To determine the amount of PAH in the supernatant, samples were prepared using fluorescein-labeled PAH (PAH-FITC), which exhibits an absorbance peak at 495 nm. After preparation and centrifugation of the sample, the supernatant was extracted, and the concentration of PAH-FITC ($C_{PAH\text{-}FITC,\ supernatant}$) was calculated using UV−vis spectroscopy with a calibration curve of PAH-FITC in 50 mM HEPES. The percentage of PAH-FITC present in the dense phase was calculated as follows:

$$\%\text{PAH-FITCincoacervate} = \left(\left(1.5\text{mM} - C_{PAH\text{-}FITC,supernatant}\right)/1.5\text{mM} \times 100\right.$$

2.8.2. Quantification of TPP. We determined the amount of TPP present in the supernatants using the vanadate-molybdate colorimetric method, commonly employed for the detection of inorganic phosphate (Pi).[42] To convert all TPP to Pi, prior acidic hydrolysis was necessary. For processing a supernatant, 1.00 mL of the sample was taken and placed in a beaker.

https://doi.org/10.1021/acs.biomac.4c01516
Biomacromolecules XXXX, XXX, XXX−XXX

Subsequently, 100 μL of 2.5 M H_2SO_4 was added, and the mixture was boiled on a hot plate for 10 min until nearly dry. The product of the hydrolysis was redissolved in deionized water to a final volume of 1.00 mL. For colorimetric analysis, 400 μL of the hydrolyzed sample was mixed with 800 μL of distilled water and 800 μL of the working reagent (20 g of ammonium molybdate, 0.5 g of ammonium metavanadate, 100 mL of sulfuric acid in 1 L of water). After 10 min, a yellow-orange color developed, which persisted over time. Once the formation of the colored complex was completed, the absorbance was measured at 420 nm by using UV−vis spectroscopy. The concentration of TPP in the supernatant was obtained by means of a calibration curve that was constructed using hydrolyzed TPP solutions of known concentrations following the same protocol. The amount of TPP in the dense phase was calculated based on the TPP concentration in the liquid phase ($C_{TPP,supernatant}$) as follows:

$$C_{TPP} - C_{TPP,supernatant} = \left(C_{TPP} - C_{PAH}\right) \times 1.5\text{mM} - C_{TPP,supernatant}$$

2.8.3. ζ-Potential and Dynamic Light Scattering Measurements. ζ-potential and dynamic light scattering (DLS) measurements were carried out with a ZetaSizer Nano (ZEN3600, Malvern, U.K.) at 20 °C using DTS1060 and DTS1060 disposable cuvettes, respectively. The protocol for sample preparation was the same as that used for turbidity measurements. Coacervate droplets' ζ-potential was determined from the electrophoretic mobility by Laser Doppler Velocimetry using a general-purpose analysis method with 100 runs for each sample. For DLS analysis (hydrodynamic diameter), PAH/TPP and PAH/BSA/TPP samples were prepared and stored for 3 h prior to measurement. A 173° backscatter angle configuration with 20 runs (10 s/run) was used for each measurement.

2.9. SAXS Measurements. SAXS experiments were performed at the Cateretê beamline of the Brazilian Synchrotron Light Laboratory (LNLS-SIRIUS, Campinas, Brazil; proposal ID: 20232697) utilizing a focused ∼8 keV X-ray beam (λ = 1.549 Å). The scattering data was captured employing a PIMEGA 540D detector housed within a vacuum chamber positioned 4 m downstream from the sample. Samples were loaded in borosilicate capillaries (1.5 mm), and their temperature during measurements was kept at 25 °C. Five frames of 10 s were acquired and averaged for each pattern. No radiation damage effects were detected during the acquisition. SAXS curves were modeled using SasView 4.2.2 software.

In all SAXS measurements, complexes were prepared using a 10X PAH concentration (compared to concentrations used in the main manuscript; i.e., C_{PAH} = 15 mM). The 10× concentration was used as SAXS patterns obtained at 1× exhibited a very low signal. Fits were performed using SasView 4.2.2. For PAH/BSA/TPP, a two-level model was used, including a polydisperse sphere (large level) with a log-normal distribution of size and a Guinier-Porod contribution (small level). The large level refers to the whole complex formed, while the small level might derive from protein molecules. The fitted parameters showed a large level with a sphere diameter of ∼88 nm with a polydispersity index (PDI) ∼0.13 while a small level presented a radius of gyration ∼2.9 nm. For PAH + TPP, a Porod contribution was used. Since the aggregate is very large, only its surface is probed by SAXS in this q-window. A Porod exponent of 3.96 was adjusted (very close to 4), indicating that the aggregate presents a smooth surface.

3. RESULTS AND DISCUSSION

3.1. Protein Loading within PAH/TPP Asymmetric Complex Coacervates. The PAH/TPP pair can be considered as a model system for an asymmetric coacervate since (i) the mixture in aqueous solution induces liquid−liquid phase separation (LLPS), (ii) both PAH and TPP are electrostatically charged species (at physiological pH), and (iii) it consists of a polycation (PAH) and a small oligomer of phosphate groups (TPP), which is a multivalent anion. To demonstrate that the PAH and TPP mixture in aqueous solution effectively undergoes LLPS, we prepared a mixture containing 1.5 mM PAH (monomer concentration) and 0.3 mM TPP in the absence of added monovalent salt and observed it under the microscope just after mixing (without centrifugation). By buffering the solution to pH = 7.4, we can assume (at least as a first approximation) that the concentration of $-NH_3^+$ ions will match the concentration of negative charges coming from TPP anions, since the degree of ionization of PAH is ∼0.8 at pH = 7.4 ($[z_+]^{pH=7.4}$ = 0.8; C_{PAH} = 1.2 mM)[43] and TPP is four times deprotonated at pH = 7.4 (pK_{a3} = 2.8, pK_{a4} = 6.5, pK_{a5} = 9.2, $[z_-]^{pH=7.4}$ = 4; C_{TPP} = 1.2 mM). As depicted in Figure 1, the combination of these components results in liquid-like coacervate droplets evenly distributed over the surface of the sample slide, confirming that the PAH and TPP mixture effectively produces the LLPS. Furthermore, when the dispersion (photograph in Figure 1) is centrifuged, a transparent dense liquid is observed at the bottom of the vial, which is again indicative of LLPS.

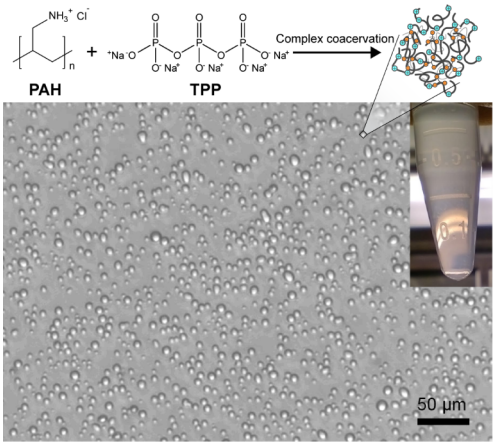

Figure 1. Optical microscopy image of an asymmetric complex coacervate composed of poly(allylamine hydrochloride) (PAH, C_{PAH} = 1.5 mM) and sodium tripolyphosphate (TPP, C_{TPP} = 0.3 mM) at pH = 7.4. The inset shows a photograph of a vial containing a freshly prepared dispersion of coacervate droplets. The top panel schematically shows the formation of the coacervate by the interaction between the charged groups of PAH and TPP.

In a recent report from our group, we investigated the conditions for the system to maintain stability as a colloidal dispersion of nanometer-sized coacervate droplets.[6] In the present work, we will not focus on the dispersion stability but rather on the capacity of the dense phase to load proteins. For this purpose, we prepared a series of solutions containing a constant concentration of PAH (C_{PAH} = 1.5 mM), a fixed protein concentration ($C_{protein}$ = 0.25 mg mL^{-1}), and varying concentrations of TPP ranging from C_{TPP} = 0 mM to C_{TPP} = 0.9 mM. In order to explore a wide range of isoelectric points (pI),

https://doi.org/10.1021/acs.biomac.4c01516
Biomacromolecules XXXX, XXX, XXX−XXX

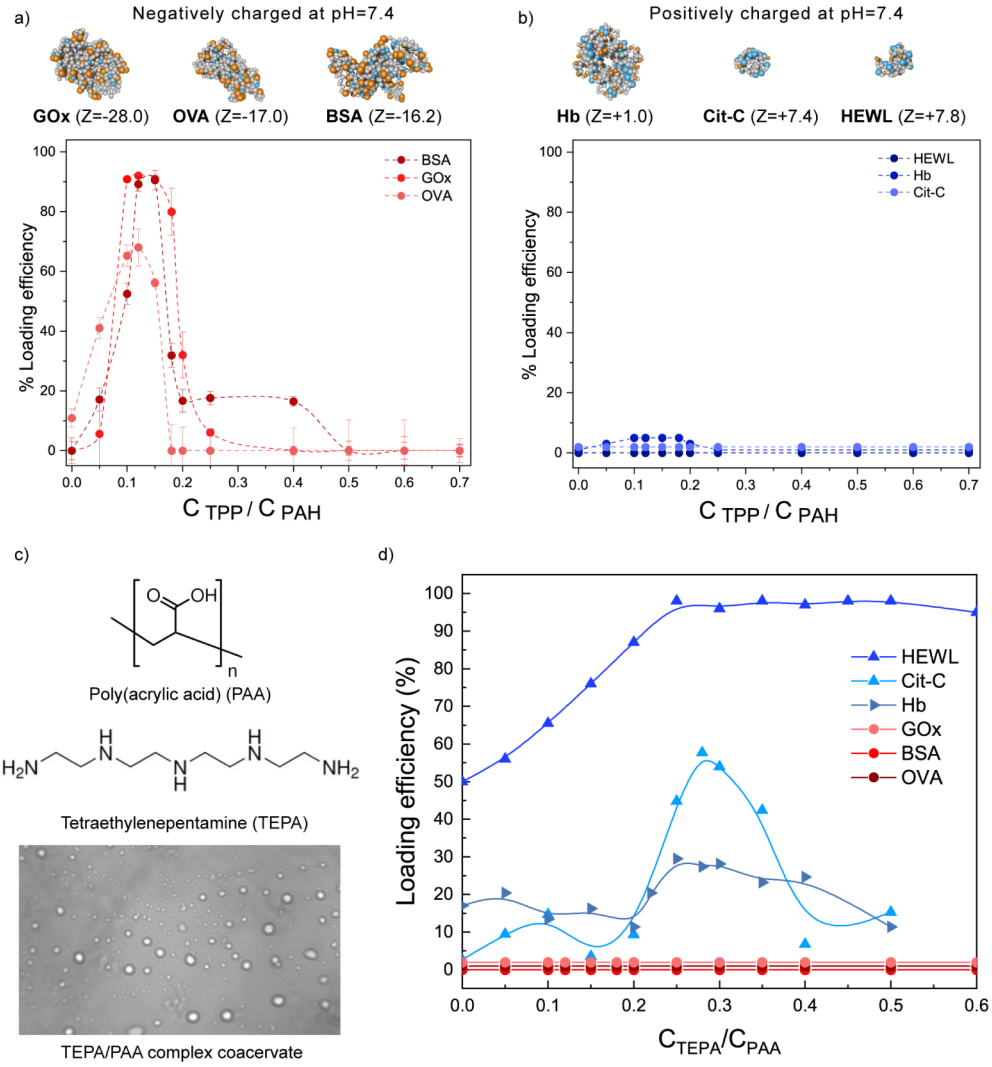

Figure 2. Top panel: Protein loading efficiency as a function of the concentration of TPP was expressed as C_{TPP}/C_{PAH} for PAH/protein/TPP systems. In all cases, C_{PAH} = 1.5 mM and $C_{protein}$ = 0.25 mg/mL. (a) PAH/GOx/TPP, PAH/OVA/TPP, and PAH/BSA/TPP (PAH/TPP + negatively charged proteins at the working pH). (b) PAH/Hb/TPP, PAH/Cit-C/TPP, and PAH/HEWL/TPP (PAH/TPP + positively charged proteins at the working pH). Each dot corresponds to the result of a protein loading efficiency experiment in an independent solution. Dashed lines are guides for the eye. Error bars represent one standard deviation (n = 3) of uncertainty. Lower panel: Protein loading characteristics for the PAA/TEPA system at pH = 7.4. (c) Chemical structures of PAA and TEPA. Optical microscopy image of an asymmetric complex coacervate formed by PAA (concentration, C_{PAA} = 1.5 mM) and TEPA (concentration, C_{TEPA} = 0.6 mM) in HEPES buffer at pH = 7.4. d) Protein loading efficiency plot expressed as a percentage relative to the total protein. The data was plotted as a function of the parameter C_{TEPA}/C_{PAA}. In all measurements, C_{PAA} = 1.5 mM and $C_{protein}$ = 0.25 mg/mL (C_{TEPA} was varied from 0 to 0.9 mM) and the solutions were buffered at pH 7.4 with HEPES buffer. Dashed lines are guides for the eye.

the proteins used in the experiment were: Ovalbumin (OVA, pI = 5.0), glucose oxidase (GOx, pI = 4.7), bovine serum albumin (BSA, pI = 5.7), hemoglobin human (Hb, pI = 7.45), cytochrome-C (Cit-C, pI = 10.0), and lysozyme (HEWL, pI = 10.9). Figure 2, top panel, illustrates the calculated protein structures and their charge distribution (see Supporting Information for calculation details). Each sample (PAH + protein + TPP) was prepared in the presence of 50 mM HEPES buffer at pH 7.4 to avoid shifts of pH during the complexation process. As a general protocol, the order of addition of reagents was (i) PAH, (ii) protein, and (iii) TPP. Each solution was stored overnight and further centrifuged to separate the liquid phase from the dense phase. The content of protein in the supernatant was obtained by means of the bicinchoninic acid (BCA) method, and the amount of loaded protein in the dense phase was calculated by difference.

Figure 2 (top panel) shows the amount of protein in the dense phase (expressed as a percentage of the total protein) as a function of the parameter C_{TPP}/C_{PAH}. For clarity of view, Figure 2a,b show the loading efficiency of proteins with pI < 7.4 and proteins with pI > 7.4, respectively. Figure S1 shows the total bulk charge of each protein as a function of pH (refer to the Supporting Information to learn about the methodology used to perform the calculations). By intersecting the plot at pH 7.4, we can estimate the charge of each protein (without considering overcharging effects due to complexation). The calculated charges (Z) per protein at pH = 7.4 were +7.8, + 7.4, + 1.0, −16.2, −17.0, and −28.0 for HEWL, Cit-C, Hb, BSA, OVA, and GOx, respectively. The first notable result that we can derive from Figure 2a,b is that while proteins with pI < 7.4 can effectively be transferred into the dense phase of coacervates, proteins with pI > 7.4 do not show appreciable loading efficiencies (at least within the range of concentrations that were

https://doi.org/10.1021/acs.biomac.4c01516
Biomacromolecules XXXX, XXX, XXX−XXX

tested). On the other hand, all samples containing proteins with pI < 7.4 present a maximum loading percentage only in a narrow window of C_{TPP}/C_{PAH}, between 0.12 and 0.2. Interestingly, within this range, the loading efficiency is close to 90%, which means that almost all protein was successfully transferred into the dense phase, independent of (i) molar weight of the protein and (ii) the number of charges per protein. In these experiments, a consistent preparation protocol was employed, where TPP was added to a premixed solution of PAH and protein. To confirm that the system's behavior is governed by the interactions between its building blocks rather than the preparation method, we conducted the same experiment using an alternative approach. In this variation, a mixture of TPP and protein was prepared first, and PAH was subsequently added with constant stirring. As shown in Figure S2, focusing on the case of BSA, the protein encapsulation profile remains largely unaffected by changes in the mixing sequence.

Since all proteins under study had a fixed concentration of 0.25 mg/mL, we can calculate the concentration of charges $[z_{protein}]$ coming from each protein by expressing the concentration of protein in mM and then multiplying that concentration by the calculated charge per protein. By doing so, we obtained $[z_{BSA}]$ = 0.061 mM, $[z_{OVA}]$ = 0.095 mM, $[z_{GOx}]$ = 0.044 mM, $[z_{Hb}]$ = 0.004 mM, $[z_{Cit\text{-}C}]$ = 0.150 mM, and $[z_{HEWL}]$ = 0.139 mM. In the absence of TPP, and assuming a degree of ionization of PAH of 0.8, the ratio of charge concentrations $[z_{PAH}]/[z_{protein}]$ is 30 for BSA/PAH, 19 for OVA/PAH, 41 for Gox/PAH, 450 for Hb/PAH, 12 for Cit-C/PAH, and 13 for HEWL/PAH. This indicates that, in all cases, the positive charges coming from PAH are always in excess with respect to the concentration of charges coming from the proteins. Considering that in order to have complexation between the protein and PAH, the formation of ion pairs between protein's charged moieties and polyelectrolyte's charged moieties must be maximized, the excess of PAH explains why there is no phase condensation between PAH and proteins in the absence of TPP. However, we do note some complex formation between PAH and OVA (10%), probably because (1) OVA and PAH are oppositely charged and (2) the ratio $[z_{PAH}]/[z_{OVA}]$ is the lowest one of the set of negatively charged proteins.

At $C_{TPP}/C_{PAH} \sim 0.15$ (maximum protein loading), and assuming 0.8 charges per monomer of PAH and 4 charges per TPP anion, the ratio between positive and negative charges $\frac{[z_{PAH}]}{[z_{TPP}]+[z_{protein}]}$ is close to 1 (1.22 ± 0.07) for all proteins, meaning that the system is now very close to charge neutralization. Here, it is worth mentioning that usually weak acids and bases tend to overcharge with respect to the soluble species due to complexation. So, $\frac{[z_{PAH}]}{[z_{TPP}]+[z_{protein}]}$ is just an estimation and should not be considered an exact value. If we inspect only the negatively charged proteins (BSA, OVA, and GOx), we see that $\frac{[z_{PAH}]}{[z_{TPP}]+[z_{protein}]} = 1.24 \pm 0.03$, which means that all three proteins are equivalent in terms of charges, despite their molar weight and charge per protein. The fact that BSA, OVA, and GOx presented the loading peak at the same C_{TPP}/C_{PAH} allows us to think that electrostatics will be a key factor to consider when presenting the mechanism of protein loading.

The BSA loading in the PAH/TPP complex at different C_{TPP}/C_{PAH} ratios (0, 0.15, 0.3, and 0.5) was evaluated by confocal fluorescence microscopy using FITC-labeled BSA. The obtained images are shown in Figure 3. First, it is observed that the

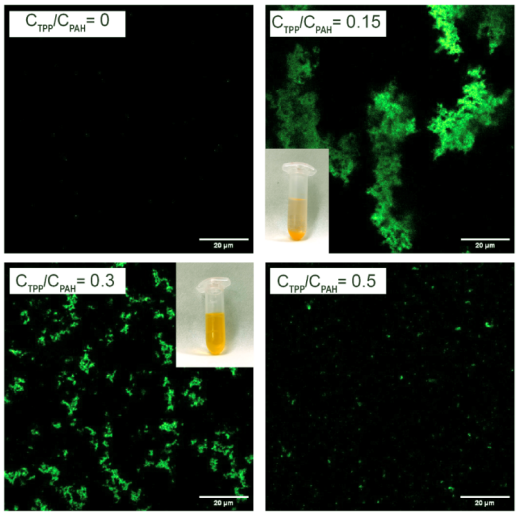

Figure 3. Confocal fluorescence micrographs of PAH/BSA-FITC/TPP complexes prepared at different C_{TPP}/C_{PAH} ratios (0, 0.15, 0.3, and 0.5). In all cases, C_{PAH} = 1.5 mM and $C_{BSA\text{-}FITC}$ = 0.25 mg/mL. C_{TPP}/C_{PAH} = 0.15 corresponds to the maximum in Figure 2a for BSA. C_{TPP}/C_{PAH} = 0 corresponds to the complex PAH/TPP without BSA-FITC and C_{TPP}/C_{PAH} = 0.5 to a PAH/BSA-FITC/TPP complex with an excess of TPP. Insets show photographs of PAH/BSA-FITC/TPP dispersions after 2 h of rest.

presence of BSA in the dense phase at different C_{TPP}/C_{PAH} ratios detected by fluorescence microscopy was consistent with the results presented in Figure 2a. By following the fluorescence emission of BSA-FITC, a maximum of BSA loading is observed at C_{TPP}/C_{PAH} = 0.15, which then decreases at 0.3 and becomes negligible at 0.5. Figure S3 shows that when C_{TPP}/C_{PAH} = 0.15, the addition of BSA provokes a massive phase condensation (which will be further confirmed by turbidity experiments). A closer inspection of the morphology of the BSA-loaded PAH/TPP complexes in Figure 3 reveals that the dense phase presents an amorphous gel-like characteristic, which differs from the spherical droplets observed for the complex without protein. According to the literature, the rheological characteristics of polyelectrolyte complexes are closely related to the internal structure of the complex and the balance between intrinsic and extrinsic ion pairs.[44−46] This balance depends on various factors, such as the nature of the counterions, the strength of electrostatic interactions, and the hydrophobicity of the polymer backbones.[22,47,48] In this case, we observed that the degree of hydration decreases upon the addition of BSA (the complex becomes less hydrated). This could indicate that the presence of BSA in the system somehow alters the internal charge arrangement compared to the protein-free analog. While this phenomenon is intriguing, it is not surprising, as we are introducing a charged macromolecule into the system, effectively creating a new system with two negatively charged short blocks and one positively charged long block.

Here, the first question is: Is the polarity (positive or negative) of the long-chain complexing agent (PAH in this case) responsible for the selectivity of the process? To answer this question, we repeated the experiment, but this time using an asymmetric complex coacervate made of poly(acrylic acid) (PAA) and tetraethylenepentamine (TEPA) (Figure 2c). PAA is a polyelectrolyte that displays negative charges at neutral pH ($pK_{a1/2}$ = 6.5).[49] On the other hand, TEPA is a small linear molecule that carries 3 secondary amine groups and 2 primary

https://doi.org/10.1021/acs.biomac.4c01516
Biomacromolecules XXXX, XXX, XXX−XXX

amine groups with pK_{a1} = 9.68, pK_{a2} = 9.10, pK_{a3} = 8.08, pK_{a4} = 4.72, and pK_{a5} = 2.98.[50] At pH = 7.4, PAA has an ionization degree of about 0.8, and TEPA carries 3 positive charges (although complexation usually induces a shift in the pK_a toward more charged species).[49] When combining PAA (C_{PAA} = 1.5 mM) and TEPA (C_{TEPA} = 0.6 mM) in aqueous solution, a liquid-like complex coacervate is formed, as can be seen in Figure 2c.

Figure 2d shows the protein loading percentage in the system PAA/TEPA under the same experimental conditions as the case of PAH/TPP. As can be seen, the system is once again selective but in the opposite direction. More specifically, the system is now able to load Cit-C, Hb, and HEWL. Moreover, the selective capturing of proteins into the dense phase is also observed in a narrow window of concentrations with C_{TEPA}/C_{PAA} between 0.2 and 0.4. As a major difference with respect to the PAH/TPP system, PAA/TEPA coacervate encapsulates HEWL even when C_{TEPA}/C_{PAA} = 0 (i.e., in the absence of TEPA). Following the same logic, we can calculate the ratio $[z_{PAA}]/[z_{protein}]$ in the absence of TEPA to determine if the system is in fact in excess of negative charges to evaluate the possibility (or not) for the PAA/protein complex to be formed. The calculated ratio $[z_{PAA}]/[z_{protein}]$ is 300 for Hb, 8 for Cit-C, and 8.6 for HEWL. This implies that, for PAA/Cit-C and PAA/HEWL, there are only 8 times more negative charges coming from PAA. This low value could be indicative of the formation of a PAA/protein complex; however, we see that PAA/HEWL retains almost 50% of the total protein, while PAA/Cit-C retains no protein in the dense phase. In line with Perry and Blocher McTigue's findings, we attribute this special feature to the presence of charge patches in HEWL that give this protein a special character as a cross-linking agent.[30] So, given that HEWL is such a strong complexing agent, it can act as a multivalent ion forming a polyelectrolyte/protein asymmetric complex coacervate in the absence of TEPA.[16,51] Also, as the PAA backbone is by nature hydrophobic, nonelectrostatic interactions could also be present between PAA and HEWL.

At C_{TEPA}/C_{PAA} = 0.275 (maximum protein partitioning), $\frac{[z_{PAA}]}{[z_{TEPA}]+[z_{protein}]} = 0.72 \pm 0.04$ for Hb, Cit-C, and HEWL, which again is close to 1 (charge neutralization). Notably, as in the PAH/TPP system, the $C_{multivalent\ ion}/C_{polyelectrolyte}$ for maximum protein uptake is placed close to charge neutralization, considering the protein just as another complexing agent.

Taken together, the results demonstrate that when there is an asymmetry in the chain length of the complex coacervate, the protein loading becomes selective. Specifically, the system can only capture proteins into the dense phase when the protein charge is opposite to that of the long-chain block (i.e., the polyelectrolyte's charge). This is a distinctive result compared to symmetric complex coacervates composed of two polymers that can encapsulate proteins of different charges by modulating the molar ratio of the building blocks.[2,5,30] In a key contribution, S. Perry and coworkers showed that when working with a chain-length symmetric system such as polyglutamic/polylysine, both negatively (pI ≪ pH) and positively (pH ≪ pI) charged proteins can be transferred into the coacervate phase when polyelectrolytes are mixed in a molar ratio close to 1 (charge neutralization) with a slight excess of the polyelectrolyte opposite to the protein's charge.[30] The authors also explored the effect of the asymmetric charge density of the complex coacervates. To do this, they substituted one or both charged homopolymers for a sequence-controlled copolymer, where half of the charged residues were replaced by neutral glycine monomers. Consequently, the resulting complex comprised a polymer with a long, fully charged chain and a copolymer consisting of two segments: one neutral and one charged. Similar to our findings, they observed that proteins with a charge opposite to that of the fully charged block were more likely to be encapsulated when mixed with the partially charged copolymer. This can be analogized to our work by considering a copolymer with half of its groups charged as equivalent to a fully charged polyelectrolyte with half the chain length. Under this assumption, Perry's results suggest that chain length asymmetry—in which the short block contains half as many monomers as the long block—shifts the system's selectivity toward capturing proteins with a charge opposite to that of the long block.

As indicated before, at pH = 7.4, the PAH has a protonation degree of about 0.8, and TPP displays 4 negative charges.[49,52] This data allows us to calculate the ratio $(C_{TPP}/C_{PAH})^{Q=0}$ for charge neutralization in the absence of cooperative ionization effects. By this, $(C_{TPP}/C_{PAH})^{Q=0} = z_{PAH}/z_{TPP} = 0.8/4 = 0.2$. If cooperative ionization takes place, then we can assume that all PAH will be completely ionized, and $(C_{TPP}/C_{PAH})^{Q}$=0 will become close to 0.25 (z_{PAH}/z_{TPP} = 1/4).[53,54] So, as a first approximation, the ratio C_{TPP}/C_{PAH} for charge neutralization will be somewhere between 0.2 and 0.25. Since the peak of protein loading is placed in the region of C_{TPP}/C_{PAH} = 0.12−0.15 (Figure 2a), the process of protein uptake by the dense phase is taking place not in the region of charge neutralization between PAH and TPP but in a region in which there is a slight excess of positive charges, coming from the ionized amine groups in PAH. These findings are aligned with what has been previously observed for symmetric coacervates, where negatively charged proteins are captured by symmetric coacervates with a slight excess of polycation (i.e., the peak of maximum encapsulation is shifted from the zero-charge position).[5,30,55] We believe that the reason for this phenomenon is that, as proteins carry negative charges, the charge neutralization of the system will be given when $\frac{[z_{PAH}]}{[z_{TPP}]+[z_{protein}]} = 1$ as demonstrated before. So, as protein concentration increases, less TPP will be needed for charge neutralization, and the peak will shift to the left (see Figure S4).

3.2. PAH/TPP Complexation in Absence of BSA. To understand the mechanism of protein uptake in asymmetric complex coacervates, we first examined the behavior of the system without the presence of added proteins. For this, we quantified both PAH and TPP in the dense phase of the PAH/TPP coacervate for different C_{TPP}/C_{PAH} ratios, maintaining C_{PAH} constant. The PAH and TPP contents in the coacervate were expressed as %PAH in the dense phase relative to the total (%PAH in coacervate) and $C_{TPP} - C_{TPP,\ supernatant}$, respectively.

Figure 4a (blue line) shows the content of PAH in the coacervate phase as a function of C_{TPP}/C_{PAH} in the absence of BSA. As observed, 90% of the total PAH is transferred into the dense phase for $C_{TPP}/C_{PAH} \geq 0.2$. In particular, at C_{TPP}/C_{PAH} = 0.2, $\%PAH_{coacervate}$ = 87% and $C_{TPP} - C_{TPP,\ supernatant}$ = 0.2 mM (Figure 4c, blue line). Given that TPP carries 4 negative charges per ion and that 90% of PAH (1.35 mM) is localized in the dense phase, the degree of protonation of PAH in the dense phase can be calculated (assuming electroneutrality in the coacervate). Consequently, the calculated degree of protonation of PAH in the dense phase is 0.59, slightly lower than the degree of protonation of free PAH at the same pH. As it would be logically expected for the degree of protonation of PAH to increase after association with anions rather than decrease, it can be asserted

https://doi.org/10.1021/acs.biomac.4c01516
Biomacromolecules XXXX, XXX, XXX−XXX

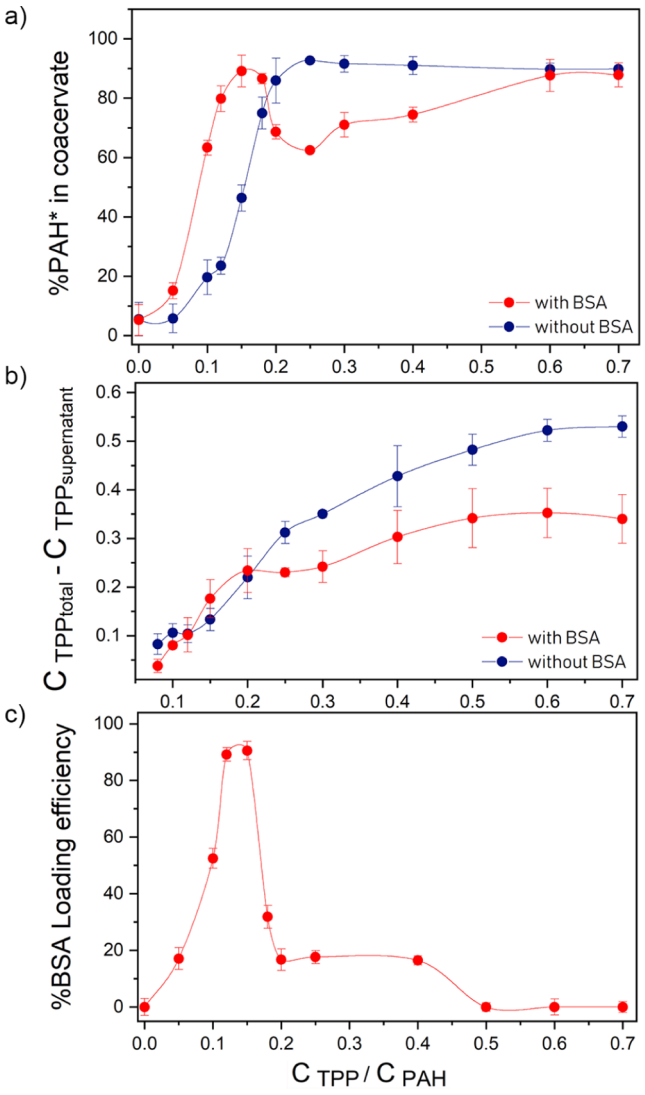

Figure 4. Quantification of the components in the dense phase of the coacervate for the PAH/TPP and PAH/BSA/TPP systems for different concentrations of TPP, expressed as C_{TPP}/C_{PAH}. In all cases, C_{PAH} = 1.5 mM and $C_{protein}$ = 0.25 mg/mL. (A) Percentage of PAH-FITC (PAH*) in the dense phase for PAH/TPP (blue dots) and PAH/BSA/TPP (red dots) coacervates. The percentage was calculated relative to the total amount of PAH* present. (B) Difference between the total concentration of TPP and the concentration of TPP in the liquid phase (indicative of the amount of TPP sequestered in the dense phase) for PAH/TPP (blue dots) and PAH/BSA/TPP (red dots) coacervates. (C) BSA loading efficiency for the PAH/BSA/TPP coacervate (data taken from Figure 2a). Each dot corresponds to an independent experiment. Lines are guides for the eye. Error bars represent one standard deviation (n = 3) of uncertainty.

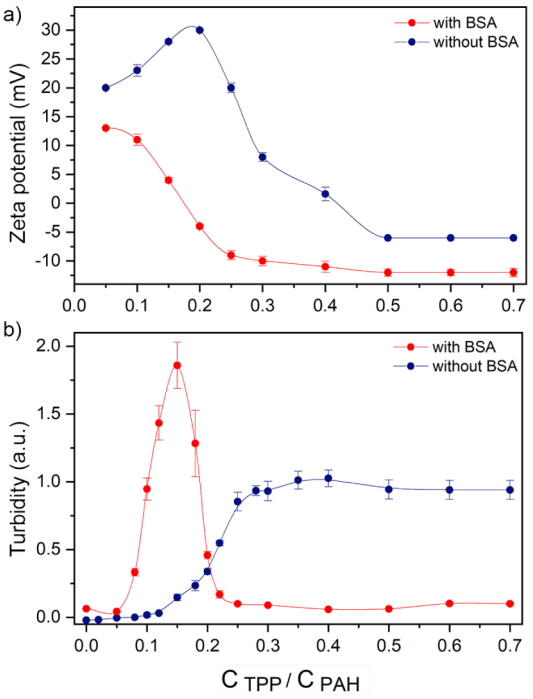

Figure 5. Evolution of the zeta potential (A) and turbidity (B) of the system for freshly prepared mixtures of asymmetric coacervates PAH/TPP (blue points) and PAH/BSA/TPP (red points) as a function of increasing C_{TPP}/C_{PAH} ratio. In both panels (A and B), the concentrations of PAH and BSA were 1.5 mM and 0.25 mg/mL, respectively. Each dot corresponds to an independent experiment. Lines are guides for the eye. Error bars represent one standard deviation of the uncertainty.

that the condition of electroneutrality in the coacervate is not met. This implies that the coacervate is somehow overcharged with a positive charge.

From this point onward, as more TPP is introduced into the system, the percentage of PAH in the dense phase remains constant while the quantity of TPP increases, reaching ~0.5 mM for C_{TPP}/C_{PAH} = 0.6. Figure 5b illustrates the evolution of the zeta potential of the coacervate droplets formed immediately after the mixing process. In this plot, it is observed that the zeta potential of the PAH/TPP system becomes zero for C_{TPP}/C_{PAH} = 0.4. If we calculate the degree of protonation of PAH at this point (knowing that $C_{TPP} - C_{TPP,\ supernatant}$ is 0.4 mM here), we obtain a value of 1.18 (~1). This implies that when C_{TPP}/C_{PAH} = 0.4, the total charge of the system is zero, and PAH is fully protonated. On the contrary, when C_{TPP}/C_{PAH} > 0.4, the zeta potential becomes negative, indicating an inversion of charge in the coacervate's overcharge due to the excess of TPP.

Taking it all together, it can be concluded that in the absence of BSA, (i) the total charge neutralization ratio is C_{TPP}/C_{PAH} = 0.4, and PAH is completely protonated; (ii) for C_{TPP}/C_{PAH} = 0.2, all PAH is complexed, and the system exhibits a positive overcharge; (iii) starting from C_{TPP}/C_{PAH} = 0.4, the excess TPP in the dense phase leads to a reversal in the overcharge sign. In the following, we will analyze the effect of the presence of BSA to gain insights into the physicochemical aspects underlying the results presented in Figure 2.

3.3. PAH/TPP Complexation in the Presence of BSA.

Figure 5b depicts the changes in turbidity as a function of C_{TPP}/C_{PAH} for both the PAH/TPP system and the ternary PAH/BSA/TPP system, with the BSA concentration fixed at 0.25 mg/mL (3.8 μM). Here we can see that, for the case without BSA, turbidity reaches a maximum at C_{TPP}/C_{PAH} = 0.25, remaining constant at higher C_{TPP}/C_{PAH} values. Instead, for the case of the ternary system, turbidity reaches a maximum at C_{TPP}/C_{PAH} = 0.15 and then decreases at higher C_{TPP}/C_{PAH} values. Notably, above C_{TPP}/C_{PAH} = 0.2 (a concentration range where the protein content in the dense phase is very low), the ternary system's turbidity attains very small values. Moreover, charge neutrality (zeta potential = 0) in the ternary system occurs at C_{TPP}/C_{PAH} close to 0.15 (Figure 5a), aligning with both the turbidity and encapsulation maxima. For C_{TPP}/C_{PAH} values greater than 0.15,

https://doi.org/10.1021/acs.biomac.4c01516
Biomacromolecules XXXX, XXX, XXX−XXX

the zeta potential takes negative values (Figure 5b), indicating an excess of negative charge in the dense phase. It is noteworthy at this point that the presence of BSA in the medium induces a shift of the zero-charge zeta potential toward lower C_{TPP}/C_{PAH} values.

Another interesting finding is that, in the presence of BSA, the amount of PAH in the dense phase exhibits a maximum at C_{TPP}/C_{PAH} = 0.15 (Figure 4a, red line), subsequently decreasing to around 60% at C_{TPP}/C_{PAH} = 0.2, and then gradually increasing to approximately 90% at C_{TPP}/C_{PAH} = 0.6. Moreover, an additional effect is observed: the quantity of TPP in the dense phase no longer increases linearly but reaches a plateau at $C_{TPP} - C_{TPP,\ supernatant} \approx 0.3$ mM (Figure 4b).

If we consider BSA simply as a multivalent negatively charged macromolecule, we might conceive that TPP and BSA compete for the complexation of PAH. When the TPP concentration is very small (approaching zero), no phase separation occurs. This implies that for a BSA concentration of 0.25 mg/mL, the PAH/BSA system does not form a coacervate. In other words, the quantity of BSA is insufficient to counterbalance the charges of PAH. As the TPP concentration increases, a phase change occurs, resulting in a three-component (PAH/BSA/TPP) coacervate formation.

When C_{TPP}/C_{PAH} = 0.15, there is a 45% increase in the amount of PAH in the dense phase due to the presence of BSA (the curve shifts to the left, Figure 4a). This difference primarily stems from having more complexing agents for the same amount of polycation. Hence, complexation must occur at lower C_{TPP}/C_{PAH} values. To prove this, we conducted turbidity measurements, but this time for different BSA concentrations, ranging from 0.1 to 0.75 mg/mL. Figure S4 shows that when BSA concentration approaches zero, the peak of maximum turbidity develops close to C_{TPP}/C_{PAH} = 0.2, which is the value of maximum complexation without protein (Figure 4a, blue line). Then, as BSA concentration is increased, the peak consistently shifts toward lower C_{TPP}/C_{PAH} values. Another interesting effect is that turbidity at the maximum increases with BSA concentration until reaching a saturation point. The increase in the maximum turbidity with BSA concentration is consistent with the idea of the formation of a ternary complex at charge stoichiometry.

At this point (C_{TPP}/C_{PAH} = 0.15), the quantity of TPP in the dense phase does not significantly differ from that of the binary coacervate (Figure 4b); however, there is now more PAH in the dense phase. This implies that, at C_{TPP}/C_{PAH} = 0.15, approximately half of the PAH is complexed with TPP, and the other half is complexed with BSA. As the zeta potential at this point is very close to zero (Figure 5a), we can also assert that all charges of PAH are paired with negative charges from TPP and BSA. This shows that the combination of TPP and BSA appears to be more effective than TPP alone in neutralizing PAH charges.

Let us now analyze the region of C_{TPP}/C_{PAH} between 0.15 and 0.2. In this range: (i) the quantity of TPP in the dense phase increases similarly to the case without BSA (Figure 4b), (ii) the amounts of BSA and PAH decrease, (iii) turbidity decreases, and (iv) the zeta potential becomes negative. As the amount of TPP in the dense phase is the same as in the BSA-free counterpart but with less PAH, it is expected for the zeta potential to become negative. The coacervate formed at C_{TPP}/C_{PAH} = 0.2 in the presence of protein, therefore, exhibits an excess of TPP anions. On the other hand, the insensitivity of the TPP curve in the coacervate to the presence of BSA could indicate that TPP tends to displace BSA in a competitive process where concentrations and charge densities are sensitive parameters. Additionally, at C_{TPP}/C_{PAH} = 0.25, ~ 40% of the PAH is in solution along with almost all of the protein. We could argue that at this point the liquid phase is composed of soluble PAH/BSA and/or PAH/BSA/TPP complexes that cannot be separated into a macroscopic phase by centrifugation. To investigate this, we subjected the PAH/BSA/TPP sample (C_{TPP}/C_{PAH} = 0.25) to centrifugation for 20 min at maximum speed and analyzed the supernatant by DLS. Figure S5 shows a single distribution of sizes centered at 63 nm, indicating the presence of soluble complexes that do not undergo coacervation. Since this phenomenon appears to be a special feature of the PAH/BSA/TPP system, we will not consider that the formation of soluble complexes at this stage of titration is a relevant piece of the mechanism. Back to Figure 4, as long as the C_{TPP}/C_{PAH} parameter increases (above 0.2), the amount of PAH in the dense phase increases, but the amount of protein does not. This suggests that as the TPP concentration increases, the soluble complexes are dissociated by TPP, directing PAH toward the dense phase.

The last region that remains to be analyzed is the region where $C_{TPP}/C_{PAH} > 0.2$. In this region, in which TPP is in excess with respect to BSA, TPP anions displace BSA completely, and the complex coacervate is finally composed of PAH and TPP. Interestingly, if we compare the turbidity with and without BSA, the addition of BSA provokes a marked decrease in turbidity (stabilization of coacervate droplets), even at $C_{TPP}/C_{PAH} > 0.5$ where no BSA is detected in the dense phase (Figure 5b). Furthermore, the presence of BSA produces a decrease in the zeta potential of the aggregates (Figure 5a). Figure 6 shows

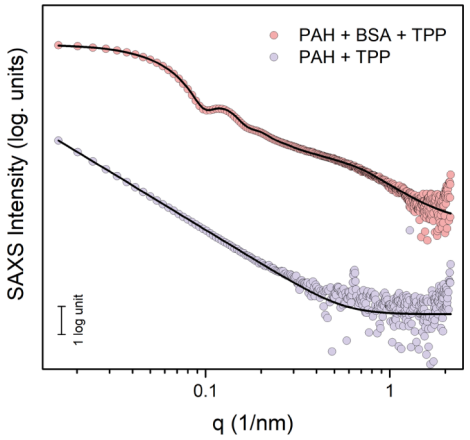

Figure 6. SAXS patterns (stacked representation) obtained for the binary (PAH + TPP; light violet dots) and ternary (PAH/BSA/TPP; light red dots) complexes prepared at C_{TPP}/C_{PAH} = 0.25 with C_{PAH} = 15 mM. Black lines represent the adjusted curves. For PAH/BSA/TPP, a two-level model including a polydisperse sphere (large level) with a log-normal distribution of size and a Guinier–Porod contribution (small level) was used. For PAH/TPP, a Porod contribution was used.

SAXS measurements of freshly prepared PAH/TPP and PAH/BSA/TPP complex coacervate dispersions at C_{TPP}/C_{PAH} = 0.25 (Figure S6 includes the SAXS pattern of BSA alone for comparison). In agreement with the turbidity results, the SAXS curve of the PAH/TPP complex corresponds to a very large aggregate with an overall size beyond the maximum dimensions probed by the experiment (above 400 nm, based on the q-window used). In contrast, the PAH/BSA/TPP complex exhibits a SAXS curve indicative of a globular object that can

https://doi.org/10.1021/acs.biomac.4c01516
Biomacromolecules XXXX, XXX, XXX−XXX

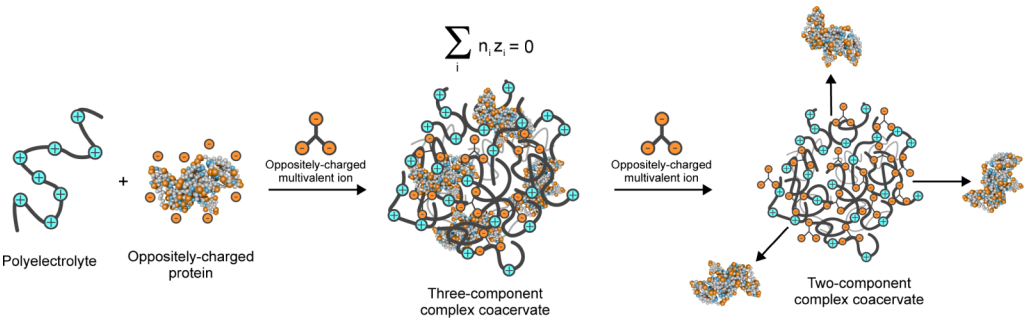

Figure 7. Simplified schematic of the protein loading mechanism in asymmetric coacervates. In the absence of a multivalent ion, phase separation does not occur, and consequently, protein uptake is not observed. Upon the addition of a multivalent ion with a charge opposite that of the polyelectrolyte, phase separation is induced, prompting the protein (which also has an opposite charge to the polyelectrolyte) to interact with the polyelectrolyte. When the total charge of the system is close to zero, a ternary complex forms, resulting in maximal protein loading. However, with the addition of excess multivalent ions, the protein is displaced and expelled into the solution, thus lowering the protein loading.

be fitted as a sphere with a diameter of approximately 88 nm and relatively low polydispersity ($\sigma \sim 11$ nm). This result was confirmed by dynamic light scattering (DLS), as shown in Figure S7. DLS measurements were taken of the coacervate droplets formed for PAH/TPP and PAH/BSA/TPP at $C_{PAH}/C_{TPP} = 0.25$ after 3 h of stabilization. The results show that the presence of BSA significantly stabilizes the coacervate droplets, reducing their hydrodynamic diameter from around 1000 nm to approximately 100 nm.

Taking this all together, we can assert that the presence of BSA increases the colloidal stability of coacervate droplets. According to the Derjaguin−Landau−Verwey−Overbeek (DLVO) theory, the stability of colloidal dispersions is influenced by the balance between attractive van der Waals interactions and repulsive electrostatic interactions. While van der Waals interactions are associated with the hydrophilicity of the colloid, electrostatic interactions are related to the surface charge. The more hydrophobic and neutral the colloids are, the lower their stability. Conversely, the more hydrophilic and charged they are, the higher their stability. Considering that BSA is a highly hydrophilic protein with a negative charge at the working pH, a possible explanation for the observed phenomenon is that BSA interacts with PAH and TPP in such a way that the resulting coacervate droplets exhibit more hydrophilic characteristics and a greater surface charge. Although it is challenging to ensure that PAH/BSA/TPP coacervate droplets are indeed more hydrophilic than PAH/TPP coacervate droplets, we can confirm that the presence of BSA increases the net surface charge, as indicated by the increased zeta potential (Figure 5b). If we then assume that the reduction in turbidity and the stabilization of coacervate droplets observed by SAXS and DLS for $C_{TPP}/C_{PAH} > 0.2$ is due to the alteration of coacervate droplet properties by BSA, it is noteworthy that this effect occurs at very high C_{TPP}/C_{PAH} values, where the amount of BSA in the dense phase is practically negligible. This could imply either that the stabilizing effect of BSA occurs with very small amounts of BSA or that when $C_{TPP}/C_{PAH} \gg 0.2$, BSA is associated with the coacervate droplets but is somehow released upon centrifugation and forced coalescence (hence its absence in the dense phase).

3.4. Mechanism of Protein Loading in Asymmetric Complex Coacervate Systems. After analyzing all the results, we can postulate that

1) Whenever there is enough distance between the working pH and the protein pI, protein uptake is given by the formation of a three-component complex coacervate in which the protein acts as a second multivalent ion (short-chain complexing agent). The formation of the ternary complex is guided by the same rules as polyelectrolyte complexes do. So, in principle, a given (and enough charged) protein can be loaded by any polyelectrolyte/multivalent salt system.
2) Because the protein acts as a short-chain complexing agent, its net charge must be opposite to that of the polyelectrolyte (long-chain complexing agent). This indicates that protein uptake is selective, allowing only proteins with charges opposite to the polyelectrolyte to be loaded.
3) Maximum protein uptake is obtained in a narrow window of $C_{multivalention}/C_{pol}$, close to charge neutralization since the formation of the ternary complex is triggered by the phase condensation between the polyelectrolyte and the multivalent ion.
4) The maximum uptake occurs when the total charge of the system ($z_{pol} + z_{multivalention} + z_{protein}$) is zero. Then, if the protein concentration is too low, the maximum uptake will occur close to the ratio of charge neutralization between the polyelectrolyte and the multivalent ion, independently on the type of the protein. As protein concentration increase, the ratio $C_{multivalention}/C_{pol}$ for maximum uptake will shift to lower values (i.e., less multivalent ions are needed to counterbalance the charge of the polyelectrolyte).
5) An excess of multivalent ions produces the displacement of the protein, lowering the protein uptake, and forming a two-component complex coacervate.

A scheme of the proposed mechanism is presented in Figure 7. The protein uptake mechanism has some major consequences that go beyond our findings: (i) an asymmetric complex coacervate system has the potential to be used as a pI-selective method for protein separation; (ii) in principle, any polyelectrolyte/multivalent ion pair can be used to load (or separate) proteins; (iii) the mechanism of formation of three-component asymmetric coacervates can be extended to other charged small molecules besides proteins. The last assumption is perhaps the most controversial, as all data presented here pertain to polyelectrolyte/protein/multivalent ion systems. As a proof of concept, we investigated a model polyelectrolyte/multivalent ion/multivalent ion system composed of PAH/$[Fe(CN)_6]^{3-}$/TPP (with $[Fe(CN)_6]^{3-}$ as a second multivalent ion). $[Fe(CN)_6]^{3-}$ has proven to be able to complex different

https://doi.org/10.1021/acs.biomac.4c01516
Biomacromolecules XXXX, XXX, XXX−XXX

polycations, such as polyethylenimine (PEI), poly(diallyldimethylammonium chloride) (PDDA), polyarginine, and polylysine.[31,56−58] In particular, for the systems PEI/$[Fe(CN)_6]^{3-}$ and PDDA/$[Fe(CN)_6]^{3-}$ we determined that the onset molar ratio $C_{Ferricyanide}/C_{Pol+}$ for complexation is about 0.2 to 0.3.[56] Thus, at $C_{Ferricyanide}/C_{Pol+}$ below 0.2, there is no complexation between $[Fe(CN)_6]^{3-}$ and polycations. To test the hypothesis, we prepared a series of solutions containing PAH with a fixed concentration of C_{PAH} = 10 mM, $[Fe(CN)_6]^{3-}$ with a fixed concentration of $C_{Ferricyanide}$ = 0.5 mM ($C_{Ferricyanide}/C_{PAH}$ = constant = 0.05), and TPP with variable concentrations, from 0 to 7 mM (C_{TPP}/C_{PAH} between 0 to 0.7). Figure S8 shows the loading percentage of $[Fe(CN)_6]^{3-}$ within the complex phase as a function of C_{TPP}/C_{PAH}. The curve shows a sharp peak centered at C_{TPP}/C_{PAH} = 0.15 with a maximum loading percentage of 100%. For C_{TPP}/C_{PAH} > 0.15, the amount of $[Fe(CN)_6]^{3-}$ within the complex phase decreases until reaching a value close to zero. Comparing the $[Fe(CN)_6]^{3-}$ loading curve with the protein loading curve (Figure S8, red dots), we can see that the behavior is almost the same. In light of these results, we confirm (at least for the case of $[Fe(CN)_6]^{3-}$) that the mechanism of formation of ternary asymmetric complex coacervates can be extended beyond proteins. Interestingly, when we evaluated a small cationic probe such as hexaammineruthenium ($[Ru(NH_3)_6]^{3+}$), no appreciable encapsulation was observed in the entire range of molar ratios (Figure S8, blue dots), proving the selectivity of the asymmetric PAH/TPP coacervates for small charged molecules. Considering that many biologically relevant metabolites/intermediaries, such as citrate, acetyl-CoA, adenosine triphosphate, or heparin, among others, carry multiple charges, the insights presented here regarding the sequestration of small multivalent molecules can serve as guidelines in the field of biomimetic condensate design.[19,59−61]

4. CONCLUSIONS

In this study, we delve into the mechanism of protein encapsulation within asymmetric coacervates comprising polyelectrolytes and multivalent ions. Unlike their symmetric counterparts, we observed a notable phenomenon: the emergence of selective protein capture in the presence of chain length asymmetry. Remarkably, only proteins bearing charges opposite to the longer polyelectrolyte block are entrapped, and this occurs within a constrained range of polyelectrolyte/multivalent ion molar ratios.

To understand this phenomenon, we conducted a systematic set of experiments to identify the composition of the coacervate's dense phase in a quantitative way, offering crucial insights into the encapsulation mechanism. Our main finding underscores the formation of a ternary asymmetric coacervate, where proteins and multivalent ions engage in a competitive interplay for polyelectrolyte complexation. Intriguingly, we observed that proteins necessitate the presence of multivalent ions to effectively complex with the polyelectrolyte and integrate into the dense phase.

This selective encapsulation mechanism, primarily driven by the charge of the longer polyelectrolyte block, holds promise for a broad spectrum of charged molecules, transcending the size and chemical composition boundaries. Our discoveries not only shed light on the fundamental principles governing protein encapsulation but also present a pioneering framework for the selective capture of multivalent ions and the synthesis of multicomponent complex coacervates. Thus, the results obtained here may have implications in different technological fields, including separation and purification technologies, microencapsulation, drug delivery, and biocatalytic microreactors. Additionally, they provide new insights into designing and exploring more realistic membrane-less organelles.

■ ASSOCIATED CONTENT

Supporting Information

The Supporting Information is available free of charge at https://pubs.acs.org/doi/10.1021/acs.biomac.4c01516.

Theoretical calculations of the net charge of proteins, studies on protein encapsulation by varying the order of reagent addition, additional confocal microscopy images, effect of protein concentration, DLS measurements of coacervate droplets, and selective encapsulation of ferricyanide ion (PDF)

■ AUTHOR INFORMATION

Corresponding Authors

Maximiliano L. Agazzi − *Instituto para el Desarrollo Agroindustrial y de la Salud, CONICET, Universidad Nacional de Río Cuarto, Río Cuarto (Córdoba) 5800, Argentina;* orcid.org/0000-0002-3065-8554; Email: magazzi@exa.unrc.edu.ar

Santiago E. Herrera − *Instituto de Química de los Materiales, Ambiente y Energía, CONICET, Universidad de Buenos Aires, CABA (Buenos Aires) 1428, Argentina;* orcid.org/0000-0002-8327-3914; Email: sherrera@qi.fcen.uba.ar

Authors

Eugenia Apuzzo − *Instituto de Investigaciones Fisicoquímicas Teóricas y Aplicadas, CONICET, Universidad Nacional de La Plata, La Plata (Buenos Aires) 1900, Argentina*

Marilina Cathcarth − *Instituto de Investigaciones Fisicoquímicas Teóricas y Aplicadas, CONICET, Universidad Nacional de La Plata, La Plata (Buenos Aires) 1900, Argentina;* orcid.org/0000-0002-1062-0954

Agustín S. Picco − *Instituto de Investigaciones Fisicoquímicas Teóricas y Aplicadas, CONICET, Universidad Nacional de La Plata, La Plata (Buenos Aires) 1900, Argentina;* orcid.org/0000-0003-4683-7319

Catalina von Bilderling − *Departamento de Tecnología y Administración, CONICET, Universidad Nacional de Avellaneda, Avellaneda (Buenos Aires) B1868, Argentina;* orcid.org/0000-0002-4913-5307

Omar Azzaroni − *Instituto de Investigaciones Fisicoquímicas Teóricas y Aplicadas, CONICET, Universidad Nacional de La Plata, La Plata (Buenos Aires) 1900, Argentina;* orcid.org/0000-0002-5098-0612

Complete contact information is available at: https://pubs.acs.org/10.1021/acs.biomac.4c01516

Notes

The authors declare no competing financial interest.

■ ACKNOWLEDGMENTS

EA and MC are fellows of CONICET; SH, MA, OA, AP, and CvB are researchers at CONICET. S.E.H. acknowledges the financial support from ANPCyT (PICT 2022-0788 and PICT 2021-0492). O.A. acknowledges the financial support from the Universidad Nacional de La Plata (PPID-X867), CONICET (PIP-0370), and ANPCyT (PICT 2017-1523 and PICT 2018-00780). A.S.P. acknowledges the financial support from

ANPCyT (PICT 2020-03923) and CONICET (PIBAA 2021-1098). The authors thank the Brazilian Synchrotron Light Laboratory (LNLS-Sirius, Campinas, Brazil) for the provision of beamtime for performing SAXS experiments at the Cateretê beamline (proposal ID: 20232697).

REFERENCES

(1) Ramos, R.; Bernard, J.; Ganachaud, F.; Miserez, A. Protein-Based Encapsulation Strategies: Toward Micro- and Nanoscale Carriers with Increased Functionality. *Small Sci.* **2022**, *2* (3), 2100095.

(2) Black, K. A.; Priftis, D.; Perry, S. L.; Yip, J.; Byun, W. Y.; Tirrell, M. Protein Encapsulation via Polypeptide Complex Coacervation. *ACS Macro Lett.* **2014**, *3* (10), 1088−1091.

(3) Blocher McTigue, W. C.; Perry, S. L. Protein Encapsulation Using Complex Coacervates: What Nature Has to Teach Us. *Small* **2020**, *16* (27), 1907671.

(4) Blocher McTigue, W. C.; Perry, S. L. Incorporation of Proteins into Complex Coacervates. *Methods In Enzymol.* **2021**, *646*, 277−306.

(5) Zhao, M.; Zacharia, N. S. Protein Encapsulation via Polyelectrolyte Complex Coacervation: Protection against Protein Denaturation. *J. Chem. Phys.* **2018**, *149* (16), 163326.

(6) Apuzzo, E.; Agazzi, M.; Herrera, S. E.; Picco, A.; Rizzo, G.; Chavero, C.; Bianchi, D.; Smaldini, P.; Cortez, M. L.; Marmisollé, W. A.; Padula, G.; Seoane, A.; Alomar, M. L.; Denofrio, M. P.; Docena, G.; Azzaroni, O. Poly(Allylamine)-Tripolyphosphate Ionic Assemblies as Nanocarriers: Friend or Foe? *ACS Appl. Bio Mater.* **2023**, *6* (11), 4714−4727.

(7) Herrera, S. E.; Agazzi, M. L.; Apuzzo, E.; Cortez, M. L.; Marmisollé, W. A.; Tagliazucchi, M.; Azzaroni, O. Polyelectrolyte-Multivalent Molecule Complexes: Physicochemical Properties and Applications. *Soft Matter* **2023**, *19*, 2013.

(8) Tirrell, M. Polyelectrolyte Complexes: Fluid or Solid? *ACS Cent. Sci.* **2018**, *4* (5), 532−533.

(9) Li, L.; Srivastava, S.; Meng, S.; Ting, J. M.; Tirrell, M. V. Effects of Non-Electrostatic Intermolecular Interactions on the Phase Behavior of pH-Sensitive Polyelectrolyte Complexes. *Macromol* **2020**, *53* (18), 7835−7844.

(10) Wang, Q.; Schlenoff, J. B. The Polyelectrolyte Complex/Coacervate Continuum. *Macromol* **2014**, *47* (9), 3108−3116.

(11) Gucht, J. V. D.; Spruijt, E.; Lemmers, M.; Stuart, M. A. C. Polyelectrolyte Complexes: Bulk Phases and Colloidal Systems. *J. Colloid Interface Sci.* **2011**, *361* (2), 407−422.

(12) Sing, C. E.; Perry, S. L. Recent Progress in the Science of Complex Coacervation. *Soft Matter* **2020**, *16* (12), 2885−2914.

(13) Srivastava, S.; Tirrell, M. V.Polyelectrolyte Complexation. In *Advances in Chemical Physics*; Wiley: Vol. *2016*, pp. 499−544. .

(14) Mountain, G. A.; Keating, C. D. Formation of Multiphase Complex Coacervates and Partitioning of Biomolecules within Them. *Biomacromolecules* **2020**, *21* (2), 630−640.

(15) Ahn, S. Y.; Obermeyer, A. C. Selectivity of Complex Coacervation in Multiprotein Mixtures. *JACS Au.* **2024**, *4*, 3800.

(16) Agazzi, M. L.; Rovey, M. F. P.; Apuzzo, E.; Herrera, S. E.; Spesia, M. B.; Oliva, M. D. L. M.; Azzaroni, O. Lysozyme/Tripolyphosphate Complex Coacervates: Properties, Curcumin Encapsulation and Antibacterial Activity. *Food Hydrocolloids* **2023**, *145*, 109134.

(17) Zhao, L.; Skwarczynski, M.; Toth, I. Polyelectrolyte-Based Platforms for the Delivery of Peptides and Proteins. *ACS Biomater. Sci. Eng.* **2019**, *5* (10), 4937−4950.

(18) Abbas, M.; Lipiński, W. P.; Wang, J.; Spruijt, E. Peptide-Based Coacervates as Biomimetic Protocells. *Chem. Soc. Rev.* **2021**, *50* (6), 3690−3705.

(19) Cakmak, F. P.; Choi, S.; Meyer, M. O.; Bevilacqua, P. C.; Keating, C. D. Prebiotically-Relevant Low Polyion Multivalency Can. Improve Functionality of Membraneless Compartments. *Nat. Commun.* **2020**, *11* (1), 5949.

(20) Nakashima, K. K.; van Haren, M. H. I.; André, A. A. M.; Robu, I.; Spruijt, E. Active Coacervate Droplets Are Protocells That Grow and Resist Ostwald Ripening. *Nat. Commun.* **2021**, *12* (1), 3819.

(21) Song, S.; Ivanov, T.; Yuan, D.; Wang, J.; da Silva, L. C.; Xie, J.; Cao, S. Peptide-Based Biomimetic Condensates via Liquid−Liquid Phase Separation as Biomedical Delivery Vehicles. *Biomacromolecules* **2024**, *25* (9), 5468−5488.

(22) Blocher, W. C.; Perry, S. L. Complex Coacervate-based Materials for Biomedicine. *WIREs Nanomed. Nanobiotechnol.* **2017**, *9* (4), No. e1442.

(23) Biswas, S.; Hecht, A. L.; Noble, S. A.; Huang, Q.; Gillilan, R. E.; Xu, A. Y. Understanding the Impacts of Molecular and Macromolecular Crowding Agents on Protein−Polymer Complex Coacervates. *Biomacromolecules* **2023**, *24* (11), 4771−4782.

(24) Devi, N.; Sarmah, M.; Khatun, B.; Maji, T. K. Encapsulation of Active Ingredients in Polysaccharide−Protein Complex Coacervates. *Adv. Colloid Interface Sci.* **2017**, *239*, 136−145.

(25) Cummings, C. S.; Obermeyer, A. C. Phase Separation Behavior of Supercharged Proteins and Polyelectrolytes. *Biochemistry* **2018**, *57* (3), 314−323.

(26) Zhou, J.; Wan, Y.; Cohen Stuart, M. A.; Wang, M.; Wang, J. Effects of Control Factors on Protein−Polyelectrolyte Complex Coacervation. *Biomacromolecules* **2023**, *24* (12), 5759−5768.

(27) Xu, Y.; Mazzawi, M.; Chen, K.; Sun, L.; Dubin, P. L. Protein Purification by Polyelectrolyte Coacervation: Influence of Protein Charge Anisotropy on Selectivity. *Biomacromolecules* **2011**, *12* (5), 1512−1522.

(28) Zhou, J.; Cai, Y.; Wan, Y.; Wu, B.; Liu, J.; Zhang, X.; Hu, W.; Cohen Stuart, M. A.; Wang, J. Protein Separation by Sequential Selective Complex Coacervation. *J. Colloid Interface Sci.* **2023**, *650*, 2065−2074.

(29) van Lente, J. J.; Claessens, M. M. A. E.; Lindhoud, S. Charge-Based Separation of Proteins Using Polyelectrolyte Complexes as Models for Membraneless Organelles. *Biomacromolecules* **2019**, *20* (10), 3696−3703.

(30) Blocher McTigue, W. C.; Perry, S. L. Design Rules for Encapsulating Proteins into Complex Coacervates. *Soft Matter* **2019**, *15* (15), 3089−3103.

(31) Coria-Oriundo, L. L.; Debais, G.; Apuzzo, E.; Herrera, S. E.; Ceolín, M.; Azzaroni, O.; Battaglini, F.; Tagliazucchi, M. Phase Behavior and Electrochemical Properties of Highly Asymmetric Redox Coacervates. *J. Phys. Chem. B* **2023**, *127* (35), 7636−7647.

(32) Bagaria, H. G.; Wong, M. S. Polyamine−Salt Aggregate Assembly of Capsules as Responsive Drug Delivery Vehicles. *J. Mater. Chem.* **2011**, *21* (26), 9454.

(33) Herrera, S. E.; Agazzi, M. L.; Cortez, M. L.; Marmisollé, W. A.; Tagliazucchi, M.; Azzaroni, O. Polyelectrolyte−Ion Complexes as Stimuli-Responsive Systems for Controlled Drug Delivery. In *Supramolecular Nanotechnology*; Wiley, 2023, pp. 729−764. .

(34) Cai, Y.; Lapitsky, Y. Analysis of Chitosan/Tripolyphosphate Micro- and Nanogel Yields Is Key to Understanding Their Protein Uptake Performance. *J. Colloid Interface Sci.* **2017**, *494*, 242−254.

(35) Su, C.-R.; Huang, Y.-Y.; Chen, Q.-H.; Li, M.-F.; Wang, H.; Li, G.-Y.; Yuan, Y. A Novel Complex Coacervate Formed by Gliadin and Sodium Alginate: Relationship to Encapsulation and Controlled Release Properties. *LWT* **2021**, *139*, 110591.

(36) Wang, J.; Abbas, M.; Wang, J.; Spruijt, E. Selective Amide Bond Formation in Redox-Active Coacervate Protocells. *Nat. Commun.* **2023**, *14* (1), 8492.

(37) Chen, X.; Chen, E.-Q.; Yang, S. Multiphase Coacervation of Polyelectrolytes Driven by Asymmetry of Charged Sequence. *Macromol* **2023**, *56* (1), 3−14.

(38) Lu, T.; Spruijt, E. Multiphase Complex Coacervate Droplets. *J. Am. Chem. Soc.* **2020**, *142* (6), 2905−2914.

(39) Qi, C.; Ma, X.; Zeng, Q.; Huang, Z.; Zhang, S.; Deng, X.; Kong, T.; Liu, Z. Multicompartmental Coacervate-Based Protocell by Spontaneous Droplet Evaporation. *Nat. Commun.* **2024**, *15* (1), 1107.

(40) Agazzi, M. L.; Herrera, S. E.; Cortez, M. L.; Marmisollé, W. A.; Tagliazucchi, M.; Azzaroni, O. Insulin Delivery from Glucose-Responsive, Self-Assembled, Polyamine Nanoparticles: Smart "Sense-and-Treat" Nanocarriers Made Easy. *Chem. - Eur. J.* **2020**, *26* (11), 2456−2463.

https://doi.org/10.1021/acs.biomac.4c01516
Biomacromolecules XXXX, XXX, XXX−XXX

(41) Lapitsky, Y. Ionically Crosslinked Polyelectrolyte Nanocarriers: Recent Advances and Open Problems. *Curr. Opin. Colloid Interface Sci.* **2014**, *19* (2), 122−130.
(42) Kitson, R. E.; Mellon, M. G. Colorimetric Determination of Phosphorus as Molybdivanadophosphoric Acid. *Ind. Eng. Chem., Anal. Ed.* **1944**, *16* (6), 379−383.
(43) Choi, J.; Rubner, M. F. Influence of the Degree of Ionization on Weak Polyelectrolyte Multilayer Assembly. *Macromolecules* **2005**, *38* (1), 116−124.
(44) Zhang, Y.; Batys, P.; O'Neal, J. T.; Li, F.; Sammalkorpi, M.; Lutkenhaus, J. L. Molecular Origin of the Glass Transition in Polyelectrolyte Assemblies. *ACS Cent. Sci.* **2018**, *4* (5), 638−644.
(45) Lalwani, S. M.; Hellikson, K.; Batys, P.; Lutkenhaus, J. L. Counter Anion Type Influences the Glass Transition Temperature of Polyelectrolyte Complexes. *Macromol* **2024**, *57* (10), 4695−4705.
(46) Sinha, N. J.; Cunha, K. C.; Murphy, R.; Hawker, C. J.; Shea, J.-E.; Helgeson, M. E. Competition between β-Sheet and Coacervate Domains Yields Diverse Morphologies in Mixtures of Oppositely Charged Homochiral Polypeptides. *Biomacromolecules* **2023**, *24* (8), 3580−3588.
(47) Comert, F.; Dubin, P. L. Liquid-Liquid and Liquid-Solid Phase Separation in Protein-Polyelectrolyte Systems. *Adv. Colloid Interface Sci.* **2017**, *239*, 213−217.
(48) Zheng, J.; Gao, Q.; Ge, G.; Wu, J.; Tang, C.; Zhao, M.; Sun, W. Sodium Chloride-Programmed Phase Transition of β-Conglycinin/Lysozyme Electrostatic Complexes from Amorphous Precipitates to Complex Coacervates. *Food Hydrocolloids* **2022**, *124*, 107247.
(49) Choi, J.; Rubner, M. F. Influence of the Degree of Ionization on Weak Polyelectrolyte Multilayer Assembly. *Macromol.* **2005**, *38* (1), 116−124.
(50) Arica, T. A.; Kuman, M.; Gercel, O.; Ayas, E. Poly(Dopamine) Grafted Bio-Silica Composite with Tetraethylenepentamine Ligands for Enhanced Adsorption of Pollutants. *Chem. Eng. Res. Des.* **2019**, *141*, 317−327.
(51) Ghimire, A.; Kasi, R. M.; Kumar, C. V. Proton-Coupled Protein Binding: Controlling Lysozyme/Poly(Acrylic Acid) Interactions with pH. *J. Phys. Chem. B* **2014**, *118* (19), 5026−5033.
(52) Huang, Y.; Lawrence, P. G.; Lapitsky, Y. Self-Assembly of Stiff, Adhesive and Self-Healing Gels from Common Polyelectrolytes. *Langmuir* **2014**, *30* (26), 7771−7777.
(53) Rathee, V. S.; Zervoudakis, A. J.; Sidky, H.; Sikora, B. J.; Whitmer, J. K. Weak Polyelectrolyte Complexation Driven by Associative Charging. *J. Chem. Phys.* **2018**, *148* (11), 114901.
(54) Katchalsky, A. Polyelectrolytes and Their Biological Interactions. *Biophys. J.* **1964**, *4* (1), 9−41.
(55) Biplab, K. C.; Nii, T.; Mori, T.; Katayama, Y.; Kishimura, A. Dynamic Frustrated Charge Hotspots Created by Charge Density Modulation Sequester Globular Proteins into Complex Coacervates. *Chem. Sci.* **2023**, *14* (24), 6608−6620.
(56) Herrera, S. E.; Agazzi, M. L.; Cortez, M. L.; Marmisollé, W. A.; Tagliazucchi, M.; Azzaroni, O. Redox-Active Polyamine-Salt Aggregates as Multistimuli-Responsive Soft Nanoparticles. *Phys. Chem. Chem. Phys.* **2020**, *22* (14), 7440−7450.
(57) Smokers, I. B. A.; van Haren, M. H. I.; Lu, T.; Spruijt, E. Complex Coacervation and Compartmentalized Conversion of Prebiotically Relevant Metabolites. *ChemSystemschem* **2022**, *4*, No. e202200004.
(58) Wang, J.; Abbas, M.; Wang, J.; Spruijt, E. Selective Amide Bond Formation in Redox-Active Coacervate Protocells. *Nat. Commun.* **2023**, *14*, 8492.
(59) Roy, P. S. Complex Coacervate-Based Materials for Biomedicine: Recent Advancements and Future Prospects. *Ind. Eng. Chem. Res.* **2024**, *63* (13), 5414−5487.
(60) Cook, A. B.; Novosedlik, S.; van Hest, J. C. M. Complex Coacervate Materials as Artificial Cells. *Acc. Mater. Res.* **2023**, *4* (3), 287−298.
(61) Deng, J.; Walther, A. Programmable ATP-Fueled DNA Coacervates by Transient Liquid-Liquid Phase Separation. *Chem* **2020**, *6* (12), 3329−3343.

https://doi.org/10.1021/acs.biomac.4c01516
Biomacromolecules XXXX, XXX, XXX−XXX